Research Square

Preprints are preliminary reports that have not undergone peer review.
They should not be considered conclusive, used to inform clinical practice,
or referenced by the media as validated information.

Preparation of a Phosphogypsum-Based Si-Ca-K-Mg Fertilizer at a Moderate Temperature and Its Remediation Mechanism in Acidic Cd-Polluted Soils

Qi Liu

liuqi6766@163.com

Huazhong Agriculture University https://orcid.org/0000-0001-9159-7444

Yuqing Chen

Xuchao Sun

Rongteng Zhao

Lanfeng Li

Weibao Xu

Yan Tang

Chunhong Yang

Wenbing Zhou

https://orcid.org/0000-0003-1952-1263

Research Article

Keywords: Phosphogypsum, Si-Ca-K-Mg fertilizer, Thermochemical conversion, Cd immobilization, Detoxification mechanism

Posted Date: June 1st, 2026

DOI: https://doi.org/10.21203/rs.3.rs-9722732/v1

License: This work is licensed under a Creative Commons Attribution 4.0 International License.
Read Full License

Version of Record: A version of this preprint was published at Plant and Soil on July 24th, 2026. See the published version at https://doi.org/10.1007/s11104-026-08930-9.

Abstract

Background and Aims

Phosphogypsum (PG) accumulation, soil acidification, and cadmium (Cd) pollution threaten agricultural sustainability. This study aimed to synthesize a Si-Ca-K-Mg fertilizer (PGF) from PG and elucidate the mechanisms by which it remediates acidic Cd-polluted soil and alleviates plant toxicity.

Methods

A phosphogypsum-based fertilizer (PGF) was synthesized via thermochemical conversion at 850°C using PG, biomass ash, and dolomite. Its efficacy was evaluated through soil incubation and lettuce (Lactuca sativa) pot experiments. Soil physicochemical properties, Cd speciation, plant physiological responses, and the subcellular distribution of Cd were systematically analyzed to identify the underlying remediation drivers.

Results

Characterization of the synthesized PGF revealed active mineral phases (Ca_2SiO_4, CaO) that neutralized soil acidity, eliminated exchangeable Al^{3+}, and enhanced the supply of available Si, Ca, Mg, and K. In soil, PGF application promoted the transformation of exchangeable Cd into Fe-Mn oxide-bound and residual fractions through precipitation and specific adsorption. In lettuce, the amendment alleviated Cd-induced growth inhibition by enhancing photosynthesis and antioxidant enzyme activities. The detoxification mechanism was attributed to the redistribution of Cd from metabolically active organelles to cell walls and vacuoles, where it was sequestered in pectin-bound and insoluble forms. Correlation analysis revealed that soil pH increase and Al^{3+} elimination were the primary drivers for restoring plant functions, while nutrient release and Cd stabilization synergistically reduced shoot Cd accumulation.

Conclusion

This study demonstrates that PGF provides a dual-benefit strategy for industrial waste utilization and remediation of polluted lands by integrating soil environmental regulation with plant physiological detoxification.

Introduction

Phosphoric acid is the core raw material for agricultural phosphorus fertilizer production (Cai et al. 2026). Approximately 90% of global phosphoric acid is produced via the wet process using phosphate rock and sulfuric acid (Yao et al. 2025). While extracting phosphoric acid, this process generates

massive amounts of an industrial byproduct, phosphogypsum (PG). For every 1 ton of phosphoric acid produced, approximately 4–6 tons of PG are generated (Liu et al. 2025b). Currently, the global cumulative stockpile of PG exceeds 7 billion tons and is growing at an annual rate of approximately 280 million tons (Zeng et al. 2026). As the world's largest phosphorus fertilizer producer, China generates about 80 million tons of PG annually, yet its comprehensive utilization rate remains below 40% (Hou et al. 2026). Due to the lack of economically viable treatment technologies, large quantities of PG are primarily stockpiled in the open air (Liu et al. 2025c). Residual impurities in PG pose environmental contamination risks through leaching (Akfas et al. 2024). In the vicinity of phosphorus chemical industrial zones, affected by ore processing and solid waste diffusion, farmlands often face the combined stress of soil acidification and Cd pollution (Xiao et al. 2026). Soil acidification not only causes exchangeable Al^{3+} and H^{+} toxicity and leads to the loss of base cations, but the accompanying H^{+} also competes with Cd^{2+} for adsorption sites on the surface of soil colloids. This promotes the transformation of Cd into a highly active exchangeable fraction, increasing the bioavailability and mobility of Cd (Cui et al. 2025). This combined stress degrades soil physicochemical properties, inhibits crop growth, and poses potential threats to human health via the food chain (Liu et al. 2026). Therefore, there is a practical need to develop technical approaches that integrate solid waste consumption with the remediation of acidic Cd-polluted soils.

Si-Ca-K-Mg fertilizers, as mineral-based amendments, show significant potential for increasing soil pH, improving nutrient balance, and reducing heavy metal activity (Li et al. 2024). In the soil environment, the released silicate can form insoluble precipitates with Cd^{2+}, while Ca^{2+} and Mg^{2+} can replace H^{+} and Al^{3+} on soil colloids through ion exchange and compete with Cd^{2+} for absorption sites on plant roots (Liu et al. 2025d). At the plant physiological level, Si participates in the synthesis of cell wall polysaccharides (Zhou et al. 2025b), and Ca^{2+} promotes pectin cross-linking (Chen et al. 2026), which helps intercept heavy metals in the apoplast. Meanwhile, Mg and K act as physiological regulators, participating in photosynthesis regulation and antioxidant system activation (Xie et al. 2026; Alharby et al. 2026). However, the preparation of traditional Si-Ca-K-Mg fertilizers predominantly relies on natural minerals like potassium feldspar and typically requires calcination temperatures exceeding 1000°C, resulting in high resource and energy consumption (Tao et al. 2022).

Rich in Ca and S, PG is a potential raw material for Si-Ca-K-Mg fertilizer production. However, its primary component, $CaSO_4$, exhibits high thermodynamic stability, with a direct thermal decomposition temperature typically exceeding 1200°C (Laasri et al. 2023). Introducing carbon-based reducing agents (such as biochar and biomass ash) to initiate carbothermic reduction can lower the decomposition activation energy of $CaSO_4$ through solid-solid or gas-solid reaction pathways, thereby making it possible to achieve the phase reconstruction of PG at lower temperatures (Zhao et al. 2026). In this process, biomass ash—another industrial solid waste—not only provides an easily activated amorphous Si source, but its residual carbon components also exert a synergistic reducing effect, further promoting the low-temperature decomposition of $CaSO_4$ (Abioye et al. 2024). The synergistic thermochemical conversion of PG, biomass ash, K_2SO_4 (K source), dolomite (Mg source), and biochar can significantly reduce the

energy consumption of fertilizer production and achieve the comprehensive utilization of multi-source solid wastes (Zhou et al. 2025a). Currently, the remediation mechanisms of moderate-temperature PG conversion products in acidic Cd-polluted soils—particularly their comprehensive effects on Cd subcellular distribution, chemical speciation transformation in plants, and soil-plant interaction networks—require further investigation.

In view of this, we hypothesized that: (1) the synergistic thermochemical conversion of PG and biomass ash at a moderate temperature could reconstruct stable $CaSO_4$ into active silicate and oxide phases, yielding a highly effective Si-Ca-K-Mg fertilizer; (2) the application of this fertilizer would ameliorate soil acidity and immobilize soil Cd through pH-dependent precipitation, specific adsorption, and competitive ion exchange; and (3) the targeted supply of Si, Ca, and base cations from the fertilizer would trigger plant physiological detoxification by promoting Cd sequestration in cell walls and vacuoles, thereby restoring photosynthetic and antioxidant functions.

To test these hypotheses, this study used PG, biomass ash, K_2SO_4, dolomite, and biochar as raw materials to prepare the Si-Ca-K-Mg fertilizer (PGF) via an 850°C moderate-temperature thermochemical conversion process. Through soil incubation and lettuce pot experiments, the remediation efficacy of PGF in acidic Cd-polluted soils and the corresponding plant physiological responses were systematically evaluated. The specific research objectives included: (1) optimizing the preparation process of PGF and elucidating its phase reconstruction mechanism; (2) evaluating the effects of PGF on soil acidity, base cation composition, and Cd chemical speciation; (3) revealing the physiological and biochemical mechanisms and subcellular compartmentation pathways by which PGF alleviates Cd toxicity in lettuce; and (4) elucidating the internal logic of soil environmental factors driving plant physiological responses based on a correlation network model. This study aims to provide a mechanistic understanding of plant-soil interactions under combined acid-metal stress and offer a theoretical foundation for the resource utilization of phosphorus chemical solid wastes in the remediation of polluted arable lands.

Materials and Methods

Experimental Raw Materials and Soils

The PG, the primary raw material used in the experiments, was obtained from Hubei Yichang Sanning Chemical Co., Ltd. (Yichang, China). Among the modifying additives, biomass ash was sourced from Hubei Huanfeng Energy Technology Co., Ltd. (Xianning, China); dolomite, biochar, and potassium sulfate were purchased from Shijiazhuang Tanchang Trading Co., Ltd. (Shijiazhuang, China). The main chemical compositions and heavy metal contents of the raw materials are detailed in Table S1. All chemical reagents were of analytical grade (Sinopharm Chemical Reagent Co., Ltd., Shanghai, China), and ultrapure water (18.2 MΩ·cm) was used throughout the experiments.

Soil samples were collected from the surface layer (0–20 cm) of two typical farmlands in Hubei Province, China. Unpolluted soil was collected from Huangpi District, Wuhan City (30°53'55.99"N,

114°17'24.89"E), while Cd-polluted soil was collected from Dongshi Town, Zhijiang City (30°21'47.14"N, 111°36'48.99"E). The sampling site for the Cd-polluted soil is adjacent to a phosphorus chemical industrial zone and a PG stockpile area, and has been subjected to severe Cd pollution due to the long-term diffusion effects of phosphate rock processing and solid waste stockpiling. The collected soil samples were air-dried indoors, cleared of plant/animal residues and gravel, ground, and passed through a 2-mm sieve. According to the Chinese Soil Taxonomy, both soils are classified as Yellow-brown soils, corresponding to Acrisols in the FAO World Reference Base for Soil Resources (WRB). The soil parent material in both areas is primarily Quaternary alluvium, with a silty clay loam surface texture. The initial physicochemical properties of the two soils are presented in Table 1. According to the Chinese "Soil Environmental Quality: Risk Control Standard for Soil Contamination of Agricultural Land (Trial)" (GB 15618 – 2018), the Cd-polluted soil has reached the severe risk control level (pH ≤ 5.5, Cd ≥ 1.5 $mg \cdot kg^{-1}$), exhibiting typical characteristics of acidic heavy metal pollution.

Table 1
Basic physicochemical properties of the tested soils

Tested soil	pH	Organic matter ($g \cdot kg^{-1}$)	available N ($mg \cdot kg^{-1}$)	available P ($mg \cdot kg^{-1}$)	available K ($mg \cdot kg^{-1}$)	Total Cd ($mg \cdot kg^{-1}$)
Unpolluted	4.55 ± 0.03	23.1 ± 0.7	59.8 ± 2.4	20.7 ± 0.6	139 ± 4	N.D.
Cd-polluted	4.48 ± 0.04	19.5 ± 0.6	50.3 ± 2.1	17.6 ± 0.5	125 ± 3	3.0 ± 0.1
Note: N.D. indicates below the instrumental detection limit.						

Optimization of the PGF Preparation Process

The PG, biomass ash, potassium sulfate, dolomite, and biochar were dried to a constant weight at 65°C, ground, and passed through a 0.15-mm sieve. Single-factor and orthogonal experiments were employed to optimize the thermochemical conversion process. First, PG, biomass ash, potassium sulfate, dolomite, and biochar were uniformly mixed at a mass ratio of 72:9:4:10:5 and calcined at constant temperatures of 650, 750, 850, 950, and 1050°C for 25 min to screen the optimal calcination temperature. Subsequently, the mixture was calcined at the optimal temperature for 25, 45, 60, 90, and 120 min to screen the optimal calcination time. Finally, four mass ratios—T1 (62:15:4:14:5), T2 (67:12:4:12:5), T3 (72:9:4:10:5), and T4 (77:6:4:8:5)—were tested under the optimal temperature and time to screen the optimal material mass ratio.

Based on the optimal parameter intervals determined by the single-factor experiments, calcination temperature, calcination time, and material mass ratio were taken as independent variables. Three adjacent gradients were selected to design a three-factor, three-level L9(3^3) orthogonal experiment

(Tables S2-S4), and the contents of SiO_2, CaO, K_2O, and MgO in the products served as comprehensive evaluation indicators to determine the optimal process parameters. All calcination experiments were conducted in a muffle furnace (TC-5-12, Hebi Metallurgical Machinery, China). Alumina crucibles containing the mixtures were heated from room temperature (25°C) to the target temperature at $10°C \cdot min^{-1}$ and held for the specified duration. The calcined products were allowed to cool naturally to room temperature within the furnace and stored in a desiccator for subsequent material characterization, soil incubation, and pot experiments.

Experimental Design

To systematically evaluate the amelioration effect of PGF on acidic soil and compare it with raw materials and conventional treatments, a 60-day soil incubation experiment was conducted in a research greenhouse at Huazhong Agricultural University. Ten treatments were established (Table 2) with three replicates each, totaling 30 incubation pots. Unpolluted soil was thoroughly mixed with the respective amendments and placed into 2.0-L polypropylene (PP) cylindrical pots (15 cm inner diameter, 13 cm height), with 1.5 kg of soil per pot. During the incubation period, the soil surface was covered with a perforated polyethylene film to minimize water evaporation. Ultrapure water was added every 24 h via weighing to maintain the soil moisture at 70% of the field water-holding capacity. Multi-point soil samples (~ 20 g) were collected using a miniature auger on days 20, 40, and 60. Samples were air-dried and passed through a 0.15-mm sieve for physicochemical analysis.

Table 2
Treatment design for soil incubation and pot experiments

Treatment	Composition and dosage (wt%)	Experiment type
CK	No amendment	Soil incubation and pot
CaO	1% Quicklime	Soil incubation
PG_1	1% Phosphogypsum	Soil incubation and pot
PG_3	3% Phosphogypsum	Soil incubation
PG_1+CaO	1% Phosphogypsum + 1% Quicklime	Soil incubation
PG_3+CaO	3% Phosphogypsum + 1% Quicklime	Soil incubation
RM_1	1% Raw Materials mixture (uncalcined)	Soil incubation and pot
RM_3	3% Raw Materials mixture (uncalcined)	Soil incubation
PGF_1	1% Si-Ca-K-Mg fertilizer	Soil incubation and pot
PGF_3	3% Si-Ca-K-Mg fertilizer	Soil incubation and pot

Note: The uncalcined raw materials mixture (RM) was physically mixed from phosphogypsum, biomass ash, potassium sulfate, dolomite, and biochar at a mass ratio of 62:15:4:14:5. The five treatments in the pot experiment were conducted in parallel in unpolluted and Cd-polluted soils.

Based on the incubation results, five representative treatments (CK, PG_1, RM_1, PGF_1, and PGF_3) were selected for a pot experiment. The pot experiment was conducted in parallel using both unpolluted and Cd-polluted soils (Table 2) to further evaluate PGF's remediation efficacy and its effects on lettuce growth and physiology. Each treatment included four replicates, totaling 40 pots. The soils were thoroughly mixed with the amendments and placed into 2.5-L polyethylene (PE) pots (18 cm top diameter, 13 cm bottom diameter, 15 cm height), containing 2.0 kg of soil per pot. To ensure the basic nutrient requirements for lettuce growth, urea (0.64 $g \cdot pot^{-1}$, pure N 150 $mg \cdot kg^{-1}$) and KH_2PO_4 (0.70 $g \cdot pot^{-1}$, pure P 80 $mg \cdot kg^{-1}$, pure K 100 $mg \cdot kg^{-1}$) were applied as basal fertilizers to all pot treatments. These were applied as aqueous solutions, uniformly mixed into the soil, and aged for one week prior to transplanting. Uniform lettuce seedlings (four true leaves, 5.00 ± 0.25 cm in height) were selected, and one seedling was transplanted per pot. The pots were cultivated in the greenhouse for 40 days. Environmental conditions were maintained at 15–20°C, 65 ± 5% relative humidity, a 14 h/10 h light/dark cycle, and a photosynthetically active radiation of 250 ± 20 $\mu mol \cdot m^{-2} \cdot s^{-1}$. Soil moisture was maintained at 70% of the field capacity by daily weighing and watering with ultrapure water.

Analytical Methods

Material Characterization

Phase compositions were analyzed using an X-ray diffractometer (XRD, D8 Advance, Bruker, Germany) with Cu K_α radiation (2θ = 5°–90°, 3°·min^{-1}). Surface functional groups were identified using a Fourier transform infrared spectrometer (FTIR, Vertex 70, Bruker, Germany). Samples were prepared via the KBr pellet method and scanned from 4000 to 400 cm^{-1} at a resolution of 2 cm^{-1}. Following gold sputtering, microscopic morphologies were observed using a field emission scanning electron microscope (SEM, SU8010, Hitachi, Japan) equipped with an energy dispersive spectrometer (EDS) for elemental mapping. N_2 adsorption-desorption isotherms were recorded on an automated surface area and porosity analyzer (ASAP 2460, Micromeritics, USA); specific surface areas and pore size distributions were calculated using the BET and BJH models, respectively. Major oxide compositions (SiO_2, CaO, K_2O, MgO) were determined using an X-ray fluorescence spectrometer (XRF, Zetium, PANalytical, Netherlands) via the pressed pellet method (15 MPa for 30 s). Total heavy metal concentrations (Hg, Cd, Pb, As, Cr) were determined using an inductively coupled plasma optical emission spectrometer (ICP-OES, 5110 VDV, Agilent, USA) following microwave digestion in an HNO_3-HF-$HClO_4$ system.

Soil Physicochemical Analysis

Soil pH and electrical conductivity (EC) were measured potentiometrically in aqueous extracts at water-to-soil ratios of 2.5:1 and 5:1 (v/w), respectively. Available Si, available N, available P, and organic matter were determined via the acetate buffer extraction-silicon molybdenum blue colorimetric method, alkaline hydrolysis diffusion method, NH_4F-HCl extraction-molybdenum antimony anti-colorimetric method, and potassium dichromate oxidation volumetric method, respectively. Exchangeable Al^{3+} and H^+ were quantified via 1 mol·L^{-1} KCl exchange-neutralization titration. Exchangeable base cations (Ca^{2+}, Mg^{2+}, K^+, Na^+) were extracted with 1 mol·L^{-1} ammonium acetate and analyzed by ICP-OES. Cation exchange capacity (CEC) was calculated as the sum of exchangeable acidity (Al^{3+} and H^+) and total exchangeable base cations (Ca^{2+}, Mg^{2+}, K^+, and Na^+). Total soil Cd was determined by ICP-OES following aqua regia microwave digestion. Soil Cd speciation was fractionated using the Tessier five-step sequential extraction method, sequentially employing $MgCl_2$, NaAc, NH_2OH·HCl, and H_2O_2-NH_4Ac to extract the exchangeable (EX), carbonate-bound (CA), Fe-Mn oxide-bound (FMO), and organic matter-bound (OM) fractions, respectively. The extracts of each fraction and the residual fraction (RES) were uniformly determined for Cd concentration by ICP-OES after microwave digestion using HNO_3 and HNO_3-HF-$HClO_4$ systems, respectively.

Plant Physiological and Quality Analyses

At harvest (9:00–11:30 AM), photosynthetic parameters were measured using a portable photosynthesis system (CIRAS-3, Hansatech, UK). The 3rd or 4th fully expanded mature leaves from the top of four replicate plants per treatment were selected to measure net photosynthetic rate (P_n), stomatal conductance (g_s), intercellular CO_2 concentration (C_i), and transpiration rate (E). Fresh leaf samples were

assayed for superoxide dismutase (SOD), peroxidase (POD), and catalase (CAT) activities using commercial colorimetric kits (Suzhou Grace Biotechnology Co., Ltd., China). Soluble sugar, ascorbic acid, and nitrate contents were determined using the anthrone colorimetric method, 2,6-dichlorophenolindophenol titration, and the salicylic acid-sulfuric acid colorimetric method, respectively.

Leaf area (LA) was estimated non-destructively by measuring the maximum leaf length (L) and width (W) and applying a linear regression model for lettuce (Rahimikhoob et al. 2023):

$$LA = 0.65 \times (L \times W) + 3.99$$

Where *L* is the maximum leaf length (cm), *W* is the maximum leaf width (cm), and *LA* is the estimated leaf area (cm^2).

Subcellular Distribution and Chemical Speciation of Cd in Plants

Dried lettuce shoot samples were microwave-digested in an HNO_3-$HClO_4$ mixture, and total Cd was determined by ICP-OES. The subcellular distribution of Cd in leaves was determined via differential centrifugation (Weigel and Jäger 1980). Fresh leaves (0.5 g) were homogenized in a pre-cooled extraction buffer (50 mmol·L^{-1} Tris-HCl, pH 7.5; 250 mmol·L^{-1} sucrose; 1.0 mmol·L^{-1} dithiothreitol). The homogenate was filtered through a 0.15-mm nylon mesh, and the filtrate was centrifuged at 2000 × g for 15 min to pellet the cell wall fraction (F1). The supernatant was further centrifuged at 12,000 × g for 30 min to pellet the organelle fraction (F2), leaving the soluble fraction (F3, primarily vacuolar contents and cytoplasmic matrix) in the supernatant. The fractions (F1, F2, and F3) were microwave-digested with HNO_3, and trace Cd concentrations were determined by inductively coupled plasma mass spectrometry (ICP-MS, 7900, Agilent, USA). The chemical speciation of Cd in leaves was determined via sequential extraction (Wu et al. 2005). An appropriate amount of dry sample powder was weighed. 80% ethanol and ultrapure water were sequentially used to extract inorganic and water-soluble Cd; 1 mol·L^{-1} NaCl was used to extract pectin- and protein-bound Cd; finally, 2% acetic acid and 0.6 mol·L^{-1} HCl were sequentially used to extract insoluble Cd. After each step, the supernatant was collected via centrifugation, and the Cd concentration was determined by ICP-MS.

Statistical Analysis

Data were processed using Microsoft Excel 2021 and expressed as means ± standard deviations (SD). Statistical analyses were performed using SPSS 31.0. Data normality and homogeneity of variance were verified using the Shapiro-Wilk and Levene tests, respectively. For data meeting these assumptions ($p > 0.05$), one-way analysis of variance (ANOVA) followed by the least significant difference (LSD) post hoc test was used to evaluate treatment differences at a significance level of $p < 0.05$. Data visualization was performed using OriginPro 2025. Orthogonal experimental data were evaluated via range analysis.

Results

Optimization and Physicochemical Characterization of PGF

Process Optimization and Nutrient Composition

Single-factor experiments and XRF analyses (Fig. 1a-c) showed the influence of thermochemical conversion parameters on the nutrient content of PGF. SiO_2 content increased continuously as the temperature rose from 650 to 1050°C. In contrast, the contents of CaO, K_2O, and MgO reached their maximum values at 850°C and subsequently decreased at higher temperatures (Fig. 1a). Regarding calcination time, maximum nutrient retention was observed at 45 min, with a decline in elemental concentrations occurring as the duration extended to 120 min (Fig. 1b). Furthermore, increasing the mass proportions of biomass ash and dolomite led to higher SiO_2 and MgO contents in the final product (Fig. 1c).

The orthogonal experiment ($L9(3^3)$) and subsequent range analysis (Tables S2-S4) identified temperature and material ratio as the most significant factors influencing SiO_2 activation and CaO conversion, respectively. Although increasing the temperature to 950°C further enhanced SiO_2 conversion, it resulted in a reduction of CaO, K_2O, and MgO contents. Based on these findings, the optimal process conditions were determined as a mass ratio of 62:15:4:14:5 (PG:biomass ash:potassium sulfate:dolomite:biochar) calcined at 850°C for 45 min. Under these conditions, the SiO_2, CaO, K_2O, and MgO contents in PGF were 11.3%, 35.3%, 3.7%, and 2.8%, respectively, exceeding the requirements for Type I fertilizers under the Chinese National Standard (GB/T 36207 – 2018). The concentrations of heavy metals (Cd, Pb, As, Cr, and Hg) were 1.52, 24.2, 3.21, 34.9, and 0.89 $mg \cdot kg^{-1}$, respectively, which were significantly below the national safety limits (Table S1).

Microstructural and Phase Evolution

The XRD analysis (Fig. 1d, e) showed that the characteristic peaks of $CaSO_4 \cdot 2H_2O$ present in the raw PG were absent in the PGF. New diffraction peaks corresponding to Ca_2SiO_4, $K_2Mg(SiO_4)$, CaO, and CaS were observed. The FTIR spectra (Fig. 1f) exhibited an asymmetric stretching vibration peak of Si-O-Si at 1100 cm^{-1} in the PGF. The SEM imaging (Fig. 1g, h) revealed a morphological transition from the regular plate-like crystals of PG to irregular porous agglomerates in PGF. The EDS mapping (Fig. 1i) indicated a uniform distribution of Si, Ca, K, and Mg across the PGF surface. The N_2 adsorption-desorption isotherms (Fig. 1j, k) showed that PG followed a Type IV isotherm with an H3 hysteresis loop, while PGF followed a Type V isotherm. The specific surface area increased from 12.6 $m^2 \cdot g^{-1}$ in PG to 14.6 $m^2 \cdot g^{-1}$ in PGF, while the average pore diameter decreased from 18.4 nm to 15.5 nm (Fig. 1l).

Effects of PGF on Soil Physicochemical Properties

Soil incubation results (Fig. 2) showed that PGF application modified the physicochemical properties of the acidic soil. Soil pH increased progressively over the 60-day period (Fig. 2a). By day 60, pH values in

the PGF_1 and PGF_3 treatments reached 7.06 and 7.62, respectively, representing increases of 45.0% and 56.5% compared to the CK. No acidification rebound was observed in the PGF treatments during the later stages of incubation. Concurrently, exchangeable Al^{3+} and H^+ in the PGF_1 and PGF_3 treatments decreased to levels below the detection limit (Fig. 2b, c). Soil EC increased following PGF application (Fig. 2d).

The PGF application also increased the soil CEC. By day 60, the CEC in PGF_1 and PGF_3 reached 14.6 and 25.9 $cmol \cdot kg^{-1}$, respectively, which were 4.76 and 8.47 times higher than the CK (3.06 $cmol \cdot kg^{-1}$) (Fig. 2e). The concentrations of exchangeable Ca^{2+}, Mg^{2+}, and K^+ increased significantly (Fig. 2f-h). In contrast, exchangeable Na^+ in PGF_1 and PGF_3 decreased to 0.26 and 0.22 $cmol \cdot kg^{-1}$, respectively, which were significantly lower than the values observed in the CK and the raw material (RM) treatments (Fig. 2i).

Regarding nutrient availability, PGF_3 increased the available Si content to 244 $mg \cdot kg^{-1}$, a 114% increase over the CK (Fig. 2j). Available N and organic matter contents decreased across all treatments over time (Fig. 2k, l). By day 60, available N was higher in PGF_1 and PGF_3 than in the CK, while the organic matter content was lower. Available P remained stable at 19.0–19.2 $mg \cdot kg^{-1}$ across the treatments (Fig. 2m).

Chemical Speciation Transformation and Immobilization of Soil Cd

In the CK treatment of the Cd-polluted soil, Cd speciation was dominated by exchangeable (EX) and carbonate-bound (CA) fractions (Fig. 3a). Following PGF_3 application, the proportions of EX and CA fractions decreased by 60.0% and 60.5%, respectively. Conversely, the Fe-Mn oxide-bound (FMO) and residual (RES) fractions increased by 406.7% and 33.3%, respectively.

Comparative analysis of unpolluted and Cd-polluted soils (Fig. 3b-k) showed that the available Si content in the PGF_3 treatment of the Cd-polluted soil (101 $mg \cdot kg^{-1}$) was 15.1% lower than that in the unpolluted soil (119 $mg \cdot kg^{-1}$) (Fig. 3b). The soil pH in the PGF_3 treatment of the Cd-polluted soil was 7.21, which was 8.27% lower than the pH observed in the unpolluted soil (7.86) (Fig. 3c). Exchangeable H^+ in the PGF_1 treatment was higher in the Cd-polluted soil than in the unpolluted soil (Fig. 3d). In the PGF_3 treatment of the Cd-polluted soil, exchangeable Al^{3+} was below the detection limit (Fig. 3e).

In the Cd-polluted soil, CEC and exchangeable Ca^{2+}, Mg^{2+}, and K^+ remained at elevated levels in the PGF_1 and PGF_3 treatments (Fig. 3f-i). The exchangeable Na^+ content in the PGF_3 treatment decreased to 0.11 $cmol \cdot kg^{-1}$, which was lower than the 0.17 $cmol \cdot kg^{-1}$ recorded in the unpolluted soil (Fig. 3j). The available P content in the PGF_3 treatment of the Cd-polluted soil was 21.4 $mg \cdot kg^{-1}$, compared to 20.5 $mg \cdot kg^{-1}$ in the CK (Fig. 3k).

Effects of PGF on Lettuce Growth, Physiology, and Quality

Lettuce Growth and Nutritional Quality

PGF application increased lettuce growth parameters, including plant height, root length, leaf area, and fresh weight (Fig. 4a-d). In unpolluted soil, PGF_1 treatment increased plant height, root length, leaf area, and fresh weight by 26.8%, 47.2%, 83.9%, and 28.6%, respectively, compared to the CK. In the Cd-polluted soil, growth in the CK was lower than in the unpolluted CK, with reductions of 6.72% in plant height, 11.1% in root length, 9.69% in leaf area, and 27.8% in fresh weight. PGF_3 application in the Cd-polluted soil increased these parameters by 25.2%, 53.9%, 55.0%, and 63.0%, respectively, relative to the polluted CK.

Regarding nutritional quality (Fig. 4e-g), Cd stress in the CK led to a 4.61% decrease in soluble sugar and a 10.3% decrease in ascorbic acid, while nitrate content increased by 6.74% compared to the unpolluted CK. In the Cd-polluted soil, PGF_3 treatment increased soluble sugar and ascorbic acid contents by 30.7% and 12.3%, respectively, and decreased nitrate content by 23.4% compared to the CK.

Photosynthetic Characteristics and Antioxidant System

Photosynthetic parameters (Fig. 4h-k) showed that in unpolluted soil, PGF_1 treatment increased the P_n, g_s, and E by 35.3%, 36.0%, and 40.3%, respectively, compared to the CK. In the Cd-polluted soil, the CK exhibited lower P_n (41.3%), g_s (4.62%), and E (15.6%) but higher C_i (2.42%) than the unpolluted CK. PGF_3 application in the Cd-polluted soil increased P_n, g_s, and E by 141%, 29.8%, and 52.7%, respectively, while C_i decreased by 16.3% compared to the polluted CK.

Antioxidant enzyme activities (Fig. 4l-n) in the Cd-polluted CK were lower than those in the unpolluted CK, with SOD, POD, and CAT activities decreasing by 23.7%, 20.5%, and 36.4%, respectively. In unpolluted soil, PGF_1 treatment increased SOD, POD, and CAT activities by 22.4%, 37.8%, and 24.7%, respectively, compared to the CK. In Cd-polluted soil, PGF_3 treatment resulted in the highest increases in SOD (47.8%), POD (53.6%), and CAT (46.8%) activities compared to the polluted CK.

Cd Accumulation and Detoxification Mechanisms in Lettuce

In the Cd-polluted soil, the Cd concentration in lettuce shoots was 0.85 $mg \cdot kg^{-1}$ in the CK treatment (Fig. 5a). PGF application reduced shoot Cd concentrations in a dose-dependent manner, with the PGF_3 treatment reaching 0.54 $mg \cdot kg^{-1}$, a 36.5% reduction compared to the CK.

Subcellular distribution analysis (Fig. 5b) showed that in the CK, Cd was distributed in the soluble fraction (55.2%), organelles (24.7%), and cell walls (20.1%). In the PGF_3 treatment, the proportion of Cd in

organelles decreased to 7.51%, while the proportions in the cell walls and soluble fraction increased to 35.1% and 57.4%, respectively.

The chemical speciation of Cd in lettuce also shifted following PGF application (Fig. 5c). In the CK, inorganic and water-soluble Cd accounted for 48.2%, while pectin- and protein-bound Cd and insoluble Cd accounted for 20.0% and 31.8%, respectively. In the PGF_3 treatment, the proportion of inorganic and water-soluble Cd decreased to 20.4%, whereas the proportions of pectin- and protein-bound Cd and insoluble Cd increased to 37.0% and 42.6%, respectively.

Correlation Analysis of Soil-Plant Interactions

Pearson correlation analysis (Fig. 6) showed that total Cd concentration, organelle Cd concentration, and the proportion of inorganic and water-soluble Cd in lettuce were negatively correlated with the net photosynthetic rate (P_n), antioxidant enzyme activities (SOD, POD, and CAT), and growth indicators (plant height and fresh weight) ($p < 0.01$). Conversely, photosynthetic parameters and antioxidant enzyme activities exhibited positive correlations with soluble sugar and ascorbic acid contents.

Mantel tests revealed that soil basic properties and acidity (pH and exchangeable Al^{3+}) were strongly correlated with the physiological indicators of lettuce (Mantel's $p \leq 0.01$, $r \geq 0.5$). Soil Cd fractions were correlated with cell wall Cd concentrations in lettuce. Additionally, soil nutrients and base cations (available Si, Ca^{2+}, and Mg^{2+} Mg^{2+}) were correlated with the photosynthetic and antioxidant systems of the plants.

Discussion

Phase Reconstruction and Microstructural Evolution of PGF

The thermochemical conversion of PG into a Si-Ca-K-Mg fertilizer (PGF) at 850°C involves a complex sequence of carbothermic reduction and solid-state reactions. The observed decline in CaO, K_2O, and MgO contents at temperatures exceeding 850°C is likely attributable to the volatilization of alkali metals or the transformation of these elements into alternative mineral phases (Li et al. 2024). The complete disappearance of $CaSO_4$ diffraction peaks at 850°C, a temperature significantly lower than its typical thermal decomposition threshold (> 1200°C), confirms the efficacy of the carbothermic reduction pathway. In this process, biochar and the residual carbon in biomass ash act as reducing agents, lowering the activation energy and thermodynamic requirements for the conversion of $CaSO_4$ into CaO and CaS (Kale et al. 1992; Karim et al. 2019; Laasri et al. 2023).

The subsequent formation of Ca_2SiO_4 and $K_2Mg(SiO_4)$ indicates that the active CaO generated from sulfate decomposition undergoes spontaneous solid-state reactions with the amorphous SiO_2 provided by the biomass ash. This process breaks the stable silicon-oxygen bond network of the raw materials

and reconstructs it into silicate phases with higher bioavailability (Xu et al. 2024; Li et al. 2025). The FTIR analysis confirmed the polycondensation of silicon-oxygen tetrahedra, which establishes a stable silicate framework that likely governs the slow-release characteristics of the nutrients (Yan et al. 2021; Hoque et al. 2024; Karmil et al. 2025).

The morphological transition from regular plate-like crystals to irregular porous agglomerates is driven by the removal of crystal water and the escape of SO_2 and CO_2 gases, which create internal gas channels and induce porosity (Zhang et al. 2025a; Hanif and Wiinikka 2026). The resulting increase in specific surface area and the formation of a complex porous network enhance the contact interface between the PGF and the soil solution. This structural evolution provides the physicochemical basis for efficient ion exchange and the immobilization of heavy metals (Zhang et al. 2025b; Wang et al. 2026a). Compared to traditional Si-Ca-K-Mg fertilizer production, which typically requires temperatures exceeding 1000°C (Tao et al. 2022), the 850°C moderate-temperature process achieves effective phase transformation while reducing energy consumption. This provides a low-carbon pathway for the treatment of phosphorus chemical byproducts, aligning with industrial emission reduction and carbon neutrality goals (Liu et al. 2025b; Hou et al. 2026)

Mechanisms of Soil Acidity Neutralization and Cd Immobilization

The application of PGF significantly modified the chemical environment of the acidic soil. The observed increase in soil pH and the elimination of exchangeable Al^{3+} and H^+ are primarily attributed to the dissolution of alkaline components (CaO) and the hydrolysis of silicate minerals (Ca_2SiO_4). Unlike traditional liming agents such as CaO, PGF exhibited a more persistent acid-buffering effect, which prevented the acidification rebound typically observed in the later stages of soil incubation (Van Der Bauwhede et al. 2024). The removal of exchangeable Al^{3+} is a critical factor in mitigating phytotoxicity in acidic soils, as Al^{3+} ions directly inhibit root elongation and nutrient uptake (Ullah et al. 2026). Furthermore, the increase in soil CEC is linked to the hydrolysis of silicate minerals, which generates additional negative charge sites on the surfaces of soil colloids (Ng et al. 2024; Marchi et al. 2026).

The immobilization of soil Cd was driven by the transformation of highly mobile fractions (exchangeable and carbonate-bound) into more stable fractions (Fe-Mn oxide-bound and residual). The elevation of soil pH promoted the precipitation of Cd^{2+} as $CdCO_3$ (Gao et al. 2025). Simultaneously, the porous structure and surface functional groups of PGF provided specific adsorption sites for Cd^{2+}, while the increased negative surface charge on colloids enhanced electrostatic adsorption (Luo et al. 2025). The reduction in available Si in Cd-polluted soil compared to unpolluted soil suggests the formation of $CdSiO_3$ precipitates, further reducing Cd bioavailability (Zhou et al. 2026). Furthermore, the stable available P content across treatments indicates that PGF application did not induce P fixation despite the high-calcium environment.

The rhizosphere microenvironment in the Cd-polluted soil exhibited lower pH and higher exchangeable H^+ compared to the unpolluted soil, likely due to the secretion of low-molecular-weight organic acids by plant roots under metal stress and the displacement of H^+ from adsorption sites by Cd^{2+} (Zhong et al. 2025; Xu et al. 2025b). Despite these acidification drivers, the alkaline components and silicate hydrolysis in PGF maintained the soil pH within a neutral range (Yan et al. 2026). Additionally, the release of Ca^{2+} and Mg^{2+} from PGF mitigated the risk of sodium accumulation by displacing Na^+ from soil colloids through competitive adsorption, thereby improving the base cation composition (Huang et al. 2022a; Zhang et al. 2025c; Kandel et al. 2026). The observed decrease in organic matter content alongside an increase in available N suggests that the improvement in soil pH and mineral nutrient supply enhanced microbial activity, thereby accelerating the mineralization of organic matter (Lin et al. 2026).

Physiological Detoxification and Subcellular Compartmentation in Lettuce

The application of PGF effectively mitigated the growth inhibition and physiological stress induced by Cd in lettuce. Cd stress typically disrupts the synthesis of carbohydrates and ascorbic acid by damaging chloroplast structures and inhibiting photosynthetic carbon assimilation (Ahmed et al. 2023; Ghouri et al. 2025). The restoration of growth parameters and nutritional quality observed in this study is attributed to the synergistic supply of Si, Ca, K, and Mg. Specifically, Mg provided by PGF serves as a central component of chlorophyll and an activator of ribulose-1,5-bisphosphate carboxylase/oxygenase (Rubisco), thereby promoting CO_2 fixation in the Calvin cycle (Xie et al. 2026; Peinado-Torrubia et al. 2026). Simultaneously, K regulates stomatal conductance and facilitates the phloem transport of photosynthates from source leaves to sink organs by driving sucrose-H^+ symporters (White and Ding 2023; Wei et al. 2025). The concurrent increase in net photosynthetic rate and decrease in intercellular CO_2 concentration indicate that PGF primarily alleviates non-stomatal limitations, enhancing the intrinsic CO_2 assimilation capacity of the plant (Tang et al. 2013).

The enhancement of the antioxidant system and the regulation of nitrogen metabolism are further critical pathways for Cd detoxification. The increased activities of SOD, POD, and CAT following PGF application facilitate the degradation of ROS and maintain intracellular redox balance (Wang et al. 2026b). Available Si released by PGF likely participates in stress signal transduction, upregulating the expression of genes related to these antioxidant enzymes and stabilizing cell membranes (Bhardwaj et al. 2023; Xu et al. 2025a). Furthermore, Si helps restore nitrogen assimilation by protecting the active centers of nitrate reductase and upregulating genes related to nitrate reductase and glutamine synthetase, which explains the observed reduction in nitrate accumulation (Feng et al. 2010; Song et al. 2025).

The environment-dependent dose effect of PGF reflects the shift in limiting factors between unpolluted and Cd-polluted soils. In unpolluted soil, the lower dose (PGF_1) optimized nutrient supply, whereas the

higher dose (PGF_3) may have induced soil salinity or ion imbalance, thereby imposing stress on the plants (Ahmad et al. 2023). However, in Cd-polluted soil, where Cd was the primary limiting factor, PGF_3 provided the maximum capacity for Cd immobilization and pH buffering, thereby resulting in the most significant restoration of physiological functions (Liu et al. 2025a).

The reduction in shoot Cd concentration is driven by a combination of rhizosphere immobilization, competitive inhibition during uptake, and internal sequestration. High concentrations of Ca^{2+} and Mg^{2+} released by PGF compete with Cd^{2+} for root surface absorption sites, restricting the transmembrane transport of Cd (Hakeem et al. 2022; Arinzechi et al. 2025). Within the plant, the redistribution of Cd from metabolically active organelles to cell walls and vacuoles represents a primary internal detoxification mechanism. Available Si enhances the synthesis of cell wall polysaccharides, such as pectin and hemicellulose (Zheng et al. 2023; Munyaneza et al. 2025), while Ca^{2+} promotes pectin cross-linking and enhances structural stability (Chen et al. 2026). These processes increase the density of carboxyl (-COO^-) binding sites, facilitating the apoplastic interception of Cd^{2+} (Riaz et al. 2023).

In the soluble fraction, the sequestration of Cd in vacuoles is mediated by sulfur-containing ligands and base cations. S supplied by PGF promotes the synthesis of glutathione and phytochelatins, which provide sulfhydryl (-SH) binding sites for Cd (Cao et al. 2023; Kumar 2025; Sun et al. 2025). These Cd-ligand complexes are subsequently transported into the vacuole via tonoplast transporters dependent on Mg^{2+} and K^+ (Sharma et al. 2025). Furthermore, K and Mg facilitate carbohydrate metabolism and organic acid synthesis, promoting the precipitation of Cd as organic acid salts within the vacuolar lumen (Huang et al. 2021; Liao et al. 2025). These mechanisms collectively drive the transformation of highly mobile inorganic and water-soluble Cd into less toxic pectin-bound, protein-bound, and insoluble fractions, thereby protecting the functional integrity of organelles.

Soil-Plant Interaction Network and Environmental Significance

The interaction model, based on Pearson correlation and Mantel tests, provides a systemic understanding of the remediation pathways facilitated by PGF. The negative correlations between organelle Cd concentration and physiological parameters (P_n, SOD, POD, and CAT) confirm that the accumulation of Cd in metabolically active regions is the primary cause of inhibited photosynthetic carbon assimilation and oxidative stress (Usman et al. 2025). Consequently, the maintenance of carbon metabolism and ROS scavenging capacity, supported by PGF application, serves as the physiological foundation for preserving lettuce biomass and nutritional quality under Cd stress (Khan et al. 2025).

Mantel tests identified soil pH and exchangeable Al^{3+} as the dominant environmental drivers influencing plant physiological responses. This indicates that the neutralization of soil acidity and the elimination of Al^{3+} toxicity are requisite conditions for reshaping the rhizosphere microenvironment and restoring plant functions in acidic soils (Varghese et al. 2022). Furthermore, the correlation between soil Cd fractions and cell wall Cd concentrations suggests that the immobilization of Cd in the soil directly promotes its

retention in non-metabolically active plant tissues, thereby reducing systemic toxicity (Huang et al. 2022b). The positive correlations between soil nutrients (available Si, Ca^{2+}, and Mg^{2+}) and the photosynthetic and antioxidant systems indicate that the elements released by PGF act as essential physiological regulators, participating in stress signaling and the upregulation of resistance mechanisms (Mukarram et al. 2022; Thakur et al. 2025).

From an environmental and economic perspective, the 850°C thermochemical conversion process utilized in this study provides a feasible technical approach for the high-value utilization of PG. By transforming industrial solid waste into a multifunctional amendment, this method simultaneously addresses soil acidification, heavy metal pollution, and nutrient deficiencies. This integrated strategy aligns with the requirements for sustainable agricultural development and the remediation of degraded arable lands (Wang et al. 2026c).

Conclusions

In this study, a Si-Ca-K-Mg fertilizer (PGF) was successfully prepared via an 850°C thermochemical conversion process using PG, biomass ash, potassium sulfate, dolomite, and biochar. This process facilitated the reconstruction of silicate mineral phases through carbothermic reduction and high-temperature solid-state reactions. The nutrient content of the prepared PGF met national standards, and the material exhibited low environmental risks. After application to soil, PGF effectively neutralized soil acidity, decreased exchangeable Al^{3+} and H^{+} to below the detection limit, and increased both the CEC and the supply of available Si, Ca^{2+}, Mg^{2+}, and K^{+}. In the Cd-polluted soil, PGF promoted the transformation of exchangeable and carbonate-bound Cd into Fe-Mn oxide-bound and residual fractions via precipitation, specific adsorption, and competitive cation exchange, thereby significantly reducing Cd bioavailability. At the plant level, the application of PGF alleviated the inhibition of Cd stress on lettuce growth, enhanced photosynthetic capacity and antioxidant enzyme activities, and improved overall nutritional quality. Its detoxification mechanism was attributed to the synergistic effect of multiple elements (Si, Ca, S, Mg, and K), which promoted the compartmentation of Cd into cell walls and vacuoles, and its transformation into pectin- and protein-bound as well as insoluble fractions. This effectively reduced Cd toxicity in metabolically active regions such as organelles. Multidimensional correlation analysis further elucidated the interactions between soil environmental regulation and plant physiological responses: the increase in soil pH and the decrease in exchangeable Al^{3+} were the primary driving forces for restoring plant functions; the stabilization of soil Cd fractions promoted the retention of Cd in non-metabolically active regions within the plant; and the release of available Si and base cations synergistically participated in the stress resistance regulation of the plant. In conclusion, PGF possesses the functions of neutralizing acidity, supplementing nutrients, and immobilizing heavy metals. This study provides a feasible technical approach for the resource utilization of phosphorus chemical solid waste and the remediation of acidic heavy metal-polluted arable lands.

Declarations

Acknowledgements

We acknowledge the technical support from the Yunnan Soil Fertilizer and Pollution Repair Engineering Research Center and the research support from the Instrument Platform of the College of Resources and Environment, Huazhong Agricultural University.

Authors' contributions

Qi Liu: Conceptualization, Data curation, Formal analysis, Investigation, Methodology, Software, Supervision, Validation, Visualization, Writing – original draft, Writing – review & editing. Yuqing Chen: Conceptualization, Data curation, Formal analysis, Investigation. Xuchao Sun: Investigation, Validation. Rongteng Zhao: Investigation, Validation. Lanfeng Li: Investigation, Validation. Weibao Xu: Investigation, Validation. Yan Tang: Investigation, Validation. Chunhong Yang: Investigation, Validation. Wenbing Zhou: Funding acquisition, Project administration, Resources, Supervision, Writing – review & editing.

Funding

This research was funded by the Fundamental Research Funds for the Central Universities of China (2662023DKPY003).

Data availability

Data will be made available on request.

Ethics approval: Not applicable.

Consent to participate: Not applicable.

Consent for publication: Not applicable.

Conflict of interest: The author declare no competing interests.

References

1. Abioye KJ, Harun NY, Sufian S, Yusuf M, Jagaba AH, Ekeoma BC, Kamyab H, Sikiru S, Waqas S, Ibrahim H (2024) A review of biomass ash related problems: Mechanism, solution, and outlook. J Energy Inst 112:101490. https://doi.org/10.1016/j.joei.2023.101490
2. Ahmad M, Rafique MI, Akanji MA, Al-Wabel MI, Al-Swadi HA, Al-Farraj ASF (2023) Silica modified biochar mitigates the adverse effects of salt and drought stress and improves safflower (*Carthamus tinctorius* L.) growth. J Soils Sediments 23(1):172–192. https://doi.org/10.1007/s11368-022-03323-8
3. Ahmed T, Masood HA, Noman M, AL-Huqail AA, Alghanem SM, Khan MM, Muhammad S, Manzoor N, Rizwan M, Qi X, Abeed AHA, Li B (2023) Biogenic silicon nanoparticles mitigate cadmium (Cd) toxicity in rapeseed (*Brassica napus* L.) by modulating the cellular oxidative stress metabolism and

reducing Cd translocation. J Hazard Mater 459:132070. https://doi.org/10.1016/j.jhazmat.2023.132070

4. Akfas F, Elghali A, Toubri Y, Samrane K, Munoz M, Bodinier J-L, Benzaazoua M (2024) Environmental assessment of phosphogypsum: A comprehensive geochemical modeling and leaching behavior study. J Environ Manage 359:120929. https://doi.org/10.1016/j.jenvman.2024.120929
5. Alharby HF, Ansabayeva A, Alamri AM, Alghamdi SA, Alhaithloul HAS, Puchkov M, Gaplaev MS, Shehata YAM, Elshamly AMS, Al-Harbi NA, Abdelkader M (2026) Humic acid and potassium synergy drives metabolic activation, antioxidant enhancement, and improved nutrient absorption in garlic plants (*Allium sativum* L.). Sci Hortic 358:114706. https://doi.org/10.1016/j.scienta.2026.114706
6. Arinzechi C, Huang P, Zhao P, Tang C, Si M, Liao Q, Wang Q, Ping Y, Li Q, Yang Z (2025) Selenium-calcium-magnesium co-application mitigates cadmium toxicity in rice: Mechanisms of cell wall detoxification and transporter gene regulation. Rhizosphere 34:101097. https://doi.org/10.1016/j.rhisph.2025.101097
7. Bhardwaj S, Sharma D, Singh S, Ramamurthy PC, Verma T, Pujari M, Singh J, Kapoor D, Prasad R (2023) Physiological and molecular insights into the role of silicon in improving plant performance under abiotic stresses. Plant Soil 486(1–2):25–43. https://doi.org/10.1007/s11104-022-05395-4
8. Cai W, Hu D, Li H, Wen H, Shi Y, Wang J, Dai Z, Yu W, Liang S, Yang J, Yuan S (2026) Covalent organic framework/PVA membranes for efficient phosphoric acid concentration via pervaporation. Desalination 617:119421. https://doi.org/10.1016/j.desal.2025.119421
9. Cao Y, Ma C, Yu H, Tan Q, Dhankher OP, White JC, Xing B (2023) The role of sulfur nutrition in plant response to metal(loid) stress: Facilitating biofortification and phytoremediation. J Hazard Mater 443:130283. https://doi.org/10.1016/j.jhazmat.2022.130283
10. Chen M, Zhang X, Chen H, Wang X, Lu S, Gou R, You S, Shu W, Xie Z, Shi R, Yu X (2026) Calcium attenuates cadmium toxicity in Cosmos bipinnatus through cell wall remodeling and metabolic regulation: A transcriptomic and physiological analysis. Environ Pollut 398:128061. https://doi.org/10.1016/j.envpol.2026.128061
11. Cui H, Han T, Yany F, Gui L, Chen B, Lei L (2025) Synergistic response of the purple soil-ryegrass system to acidification and cadmium pollution. Pedosphere :S1002016025000578. https://doi.org/10.1016/j.pedsph.2025.06.016
12. Feng J, Shi Q, Wang X, Wei M, Yang F, Xu H (2010) Silicon supplementation ameliorated the inhibition of photosynthesis and nitrate metabolism by cadmium (Cd) toxicity in *Cucumis sativus* L. Sci Hortic 123(4):521–530. https://doi.org/10.1016/j.scienta.2009.10.013
13. Gao X, Chen X, Shu Y, Chen K, Gao G, Liu X, Huang Q, Wang L, Sun Y, Zhao Y, Liang X (2025) Mercapto-modified layered double hydroxide: High-efficiency emerging amendment for cadmium immobilization in cadmium-contaminated acidic and alkaline soil. J Hazard Mater 498:139788. https://doi.org/10.1016/j.jhazmat.2025.139788
14. Ghouri F, Jin J, Ali S, Zhong M, Liu J, Xia W, Jin F, Shahid MQ (2025) Metabolomic, biochemical, and cytological observations reveal β-Pinene's protective effects against cadmium toxicity in salt-

tolerant rice. J Environ Manage 385:125655. https://doi.org/10.1016/j.jenvman.2025.125655

15. Hakeem KR, Alharby HF, Pirzadah TB (2022) Exogenously applied calcium regulates antioxidative system and reduces cadmium-uptake in Fagopyrum esculentum. Plant Physiol Biochem 180:17–26. https://doi.org/10.1016/j.plaphy.2022.03.011
16. Hanif I, Wiinikka H (2026) Calcination of $CaCO_3$ and the subsequent sintering/densification of CaO directly visualized with in-situ SEM. Mater Chem Phys 356:132296. https://doi.org/10.1016/j.matchemphys.2026.132296
17. Hoque RA, Yadav M, Hazarika A (2024) Sulfur and magnesium-based nanofertilizer: synthesis, characterization, and applications. In: Nanofertilizer Synthesis. Elsevier, pp 195–212
18. Hou H, Yang Y, Di Z, Wu H, Cheng F, Xu H (2026) Tracking the pattern of material metabolism and environmental impacts of phosphogypsum utilization in China. J Clean Prod 557:148223. https://doi.org/10.1016/j.jclepro.2026.148223
19. Huang X, Wang C, Zhao Y, Sun C, Hu D (2021) Mechanisms and regulation of organic acid accumulation in plant vacuoles. Hortic Res 8(1):227. https://doi.org/10.1038/s41438-021-00702-z
20. Huang L, Liu Y, Ferreira JFS, Wang M, Na J, Huang J, Liang Z (2022a) Long-term combined effects of tillage and rice cultivation with phosphogypsum or farmyard manure on the concentration of salts, minerals, and heavy metals of saline-sodic paddy fields in Northeast China. Soil Tillage Res 215:105222. https://doi.org/10.1016/j.still.2021.105222
21. Huang Y, Huang B, Shen C, Zhou W, Liao Q, Chen Y, Xin J (2022b) Boron supplying alters cadmium retention in root cell walls and glutathione content in Capsicum annuum. J Hazard Mater 432:128713. https://doi.org/10.1016/j.jhazmat.2022.128713
22. Kale BB, Pande AR, Gokarn AN (1992) Studies in the carbothermic reduction of phosphogypsum. Metall Trans B 23(5):567–572. https://doi.org/10.1007/BF02649716
23. Kandel DR, Gaudel P, Poudel MB, Yun W, Lee J (2026) Single- and multi-metal engineered, functionalized hybrid biochars for heavy metal adsorption: synthesis, structure-function relationships, and coordination mechanisms. Coord Chem Rev 555:217521. https://doi.org/10.1016/j.ccr.2025.217521
24. Karim AA, Kumar M, Mohapatra S, Singh SK, Panda CR (2019) Co-plasma processing of banana peduncle with phosphogypsum waste for production of lesser toxic potassium–sulfur rich biochar. J Mater Cycles Waste Manag 21(1):107–115. https://doi.org/10.1007/s10163-018-0769-7
25. Karmil FZ, Hassoune J, El Alaoui-Belghiti H (2025) Organic-modified geopolymer nanosheet for efficient phosphorus removal from contaminated media and its potential reuse as a slow-release fertilizer. Environ Res 287:123035. https://doi.org/10.1016/j.envres.2025.123035
26. Khan Z, Duan S, Xianting F, Ahmad S, Jin C, Yang C, Khan MN, Zhang K, Shen H (2025) Novel AP-SNPs mitigate cadmium stress by regulating carbon-nitrogen metabolism and antioxidant defense system in rice. J Integr Agric :S209531192500187X. https://doi.org/10.1016/j.jia.2025.07.009
27. Kumar P (2025) Role of glutathione in heavy metal detoxification. In: Heavy Metal Toxicity and Neurodegeneration. Elsevier, pp 203–224

28. Laasri F, Carrillo Garcia A, Latifi M, Chaouki J (2023) Reaction mechanism of thermal decomposition of Phosphogypsum. Waste Manag 171:482–490. https://doi.org/10.1016/j.wasman.2023.09.035
29. Li Y, Hu T, Xiang A, Liu K, Zhang G (2024) Molybdenum tailings calcination for phase composition of Si-Ca-K-Mg fertilizers: Modification of phase transformation and its effects on plant growth. Chem Eng J 493:152726. https://doi.org/10.1016/j.cej.2024.152726
30. Li Y, Huang Z, Chai L, Wang Y, Wang X, Ke Y, Peng C, Min X (2025) Cleaner zinc extraction from high silica-calcium oxygen-sulfur mixed lead-zinc concentrates with calcium and sulfur conservation. Process Saf Environ Prot 203:107820. https://doi.org/10.1016/j.psep.2025.107820
31. Liao Q, Xiao H, Chen L, Shen C, Wang B, Zhou W, Fu H, Zheng Z, Huang B, Xin J, Huang Y (2025) Potassium alters cadmium accumulation and translocation by regulating root cell wall biosynthesis in Brassica napus. Sci Hortic 339:113833. https://doi.org/10.1016/j.scienta.2024.113833
32. Lin J, Chen Y, Lai J, Peng J, Wang X (2026) Influences and underlying mechanisms of substituting chemical nitrogen fertilizer with different organic amendments on soil nitrogen mineralization in red soil. Appl Soil Ecol 221:106925. https://doi.org/10.1016/j.apsoil.2026.106925
33. Liu Q, Sun X, Wang S, Zhao R, Li L, Zhou J, Bao L, Zhou W, Zhang N (2025a) Impacts of Humic Acid and Potassium Fulvate on Cadmium and Lead Accumulation and Translocation in Maize (*Zea mays* L.) Grown in Co-Contaminated Soil. Agriculture 15(19):2064. https://doi.org/10.3390/agriculture15192064
34. Liu X, Wu C, Lv W, Dong E, Fu S, Zhu J, Feng Y, Wang S, Chen Y, Liu K, Yu R (2025b) Stepping into the era of all-solid waste and low carbon: Phosphogypsum and other solid wastes cooperatively construct green buildings. Constr Build Mater 486:141926. https://doi.org/10.1016/j.conbuildmat.2025.141926
35. Liu Y, He D, Zou H, Chen Z, Xue S (2025c) Utilization and treatment of phosphogypsum: Environmental impacts and resource potential. J Environ Sci :S1001074225008009. https://doi.org/10.1016/j.jes.2025.12.018
36. Liu Z, Ren Z, Wang L, Liu S (2025d) Solidification/stabilization mechanism of compound heavy metal cations by phosphogypsum slag composite. Sci China Technol Sci 68(7):1720501. https://doi.org/10.1007/s11431-025-2941-y
37. Liu Q, Wang S, Sun X, Zhou J, Bao L, Li L, Zhao R, Zhou W, Zhang N (2026) Modulating Potentially Toxic Element (PTE) Bioavailability and Maize Tissue Distribution in Co-Contaminated Farmland: A Comparative Evaluation of Seven Commercial Amendments. Agriculture 16(7):785. https://doi.org/10.3390/agriculture16070785
38. Luo J, Cai Y, Yu J, Huang J, Yan J (2025) Phosphate-modified biochar- mineral-based composites for heavy metal removal in acidic environments: Development and efficiency. Appl Clay Sci 276:107924. https://doi.org/10.1016/j.clay.2025.107924
39. Marchi G, Soares JPG, De Souza Martins É, Krahl LL, De Carvalho AM, Dos Santos LF, Da Silva PB, De Freitas EM (2026) Impact of Silicate Agrominerals on Charge Generation in Cerrado Soil. In: De

Souza Martins É, Huff Theodoro S (eds) Soil Remineralizers and Silicate Fertilizers. Springer Nature Switzerland, Cham, pp 69–96

40. Mukarram M, Petrik P, Mushtaq Z, Khan MMA, Gulfishan M, Lux A (2022) Silicon nanoparticles in higher plants: Uptake, action, stress tolerance, and crosstalk with phytohormones, antioxidants, and other signalling molecules. Environ Pollut 310:119855. https://doi.org/10.1016/j.envpol.2022.119855
41. Munyaneza V, Zhang W, Haider S, Ali A, Kant S, Xu F, Wang C, Wang S, Cai H, Shi L, Ding G (2025) Silicon dioxide nanoparticles mitigate aluminum toxicity in Brassica napus via cell wall modification, reduced aluminum accumulation, and enhanced antioxidant defense. Pedosphere :S1002016025000529. https://doi.org/10.1016/j.pedsph.2025.06.011
42. Ng JF, Ahmed OH, Omar L, Jalloh MB, Kwan YM, Musah AA, Chowdhury AJK (2024) Improving pH buffering capacity of an acid soil to regulate nutrient retention and mitigate water pollution using Calciprill and sodium silicate. Desalination Water Treat 319:100491. https://doi.org/10.1016/j.dwt.2024.100491
43. Peinado-Torrubia P, Pons-Perpinyà J, Clemente-Moreno MJ, Gago J, Colmenero-Flores JM, López-Serrano L (2026) The role of the “overlooked” elements magnesium and chloride for improving photosynthesis and crop water-use efficiency in plants. Plant Soil. https://doi.org/10.1007/s11104-026-08384-z
44. Rahimikhoob H, Delshad M, Habibi R (2023) Leaf area estimation in lettuce: Comparison of artificial intelligence-based methods with image analysis technique. Measurement 222:113636. https://doi.org/10.1016/j.measurement.2023.113636
45. Riaz M, Kamran M, Fahad S, Wang X (2023) Nano-silicon mediated alleviation of Cd toxicity by cell wall adsorption and antioxidant defense system in rice seedlings. Plant Soil 486(1–2):103–117. https://doi.org/10.1007/s11104-022-05588-x
46. Sharma R, Kumar D, Parkirti P, Singh A, Sharma A, Langeh K, Singh A, Sharma M, Mir NR, Khajuria A, Kapoor N, Bhardwaj R, Ohri P (2025) Membrane transporters in Plants: Key players in abiotic and biotic stress tolerance and nutritional transport. Plant Physiol Biochem 227:110084. https://doi.org/10.1016/j.plaphy.2025.110084
47. Song J, Sun Z, Saud S, Fahad S, Nawaz T (2025) Exploring the deleterious effects of heavy metal cadmium on antioxidant defense and photosynthetic pathways in higher plants. Plant Stress 15:100716. https://doi.org/10.1016/j.stress.2024.100716
48. Sun Y, Jiang T, Sun L, Qin Q, Yang S, Wang J, Sun S, Xue Y (2025) Phosphorus and sulphur crosstalk in cereals: Unraveling the molecular interplay, agronomic impacts on yield and heavy metal tolerance. Plant Physiol Biochem 223:109838. https://doi.org/10.1016/j.plaphy.2025.109838
49. Tang L, Ying R, Jiang D, Zeng X, Morel J, Tang Y, Qiu R (2013) Impaired leaf CO_2 diffusion mediates Cd-induced inhibition of photosynthesis in the Zn/Cd hyperaccumulator Picris divaricata. Plant Physiol Biochem 73:70–76. https://doi.org/10.1016/j.plaphy.2013.09.008

50. Tao L, Guo L, Liu C, Ma X, Ma H (2022) Activate nutrients access to plants as multiphase slow-release fertilizers by sintering reaction in $K_2O–MgO–Al_2O_3–SiO_2$ system using K-feldspar as a major source. J Clean Prod 370:133511. https://doi.org/10.1016/j.jclepro.2022.133511
51. Thakur PP, Jadhav PV, Dasgupta D, Mote G, Bhagat R, Kale PB, Mane SS, Kharche V, Deshmukh R, Sonah H, Dani RG (2025) Mineral nutrient acquisition under stress: Sensing, signaling, and transportation. Plant Sci 360:112702. https://doi.org/10.1016/j.plantsci.2025.112702
52. Ullah S, Han X, Ali I, Yang M (2026) Agroforestry systems improve phosphorus bioavailability and reshape soil fungal communities in acidic forest soils by mitigating aluminum-induced stress. Ind Crops Prod 240:122570. https://doi.org/10.1016/j.indcrop.2025.122570
53. Usman S, Noreen Z, Shah AA (2025) Melatonin-loaded silica nanoparticles alleviate cadmium toxicity in *Solanum lycopersicum* L. by regulating chlorophyll fluorescence, gas-exchange, physio-biochemical attributes, antioxidant defense and metal-uptake. Plant Physiol Biochem 229:110675. https://doi.org/10.1016/j.plaphy.2025.110675
54. Van Der Bauwhede R, Muys B, Vancampenhout K, Smolders E (2024) Accelerated weathering of silicate rock dusts predicts the slow-release liming in soils depending on rock mineralogy, soil acidity, and test methodology. Geoderma 441:116734. https://doi.org/10.1016/j.geoderma.2023.116734
55. Varghese EM, Kour B, Ramya S, Kumar NS, Jisha MS, Ramakrishnan B (2022) Rhizosphere microbe-mediated alleviation of aluminum and iron toxicity in acidic soils. In: Rhizosphere Engineering. Elsevier, pp 499–526
56. Wang D, Mu B, Zhao F, Liu Y, Zhu Y, Wang A (2026a) Sustainable synthesis of phosphate/silicate/biochar composites derived from oil shale semi-coke waste for efficient adsorption and passivation of heavy metals. J Environ Chem Eng 14(1):121116. https://doi.org/10.1016/j.jece.2026.121116
57. Wang F, Wei Z, Yao S, Xie S, Wang L, Ji J (2026b) The role of melatonin in enhancing cadmium stress tolerance in okra: Physiological and biochemical insights. Plant Soil. https://doi.org/10.1007/s11104-026-08358-1
58. Wang T, Chen C, Jiang X, Zhao Y, Zhao Y, Li X, Wang L, Wanghan J, Ma W, Liu Z (2026c) Current research status and emerging trends of phosphogypsum resource utilization: A review combined with bibliometric analysis. J Environ Chem Eng 14(2):121807. https://doi.org/10.1016/j.jece.2026.121807
59. Wei J, Hu K, Liu M, Liu Y, Tian W, Zhou Y, Fan L, Wang Y, Wang Y (2025) Guard cells on the adaxial and abaxial leaf surfaces use different compositions of potassium ion channels to drive light-induced stomatal opening. Nat Plants 11(7):1260–1269. https://doi.org/10.1038/s41477-025-02026-5
60. Weigel HJ, Jäger HJ (1980) Subcellular Distribution and Chemical Form of Cadmium in Bean Plants. Plant Physiol 65(3):480–482. https://doi.org/10.1104/pp.65.3.480

61. White PJ, Ding G (2023) Long-distance transport in the xylem and phloem. In: Marschner's Mineral Nutrition of Plants. Elsevier, pp 73–104
62. Wu F, Dong J, Qian Q, Zhang G (2005) Subcellular distribution and chemical form of Cd and Cd–Zn interaction in different barley genotypes. Chemosphere 60(10):1437–1446. https://doi.org/10.1016/j.chemosphere.2005.01.071
63. Xiao L, Feng P, Liang Y, Xia B, Ye Y, Liu H, Zhao W, Li Z, Cheng K, Chen J (2026) A machine learning framework bridging heavy metal contamination and human health risks in agricultural soils of the Yangtze River Delta (2001–2030). J Hazard Mater 505:141527. https://doi.org/10.1016/j.jhazmat.2026.141527
64. Xie R, Gao J, Wu C, Guo J, Cheng Q, Wang H, Liang T, Lu J, Zheng C, Wu L, Chen L, Chen S, Li W (2026) Magnesium deficiency limits electron transport efficiency and photosynthesis, and induces oxidative stress in tobacco. Plant Sci 362:112844. https://doi.org/10.1016/j.plantsci.2025.112844
65. Xu P, Liu W, Li H, Chen Y (2024) Thermal decomposition mechanism and characterization of phosphogypsum in suspension under multifactor coupling effect. Case Stud Constr Mater 20:e02861. https://doi.org/10.1016/j.cscm.2024.e02861
66. Xu J, Shao Y, Rao X, Tang J, Rensing C, Alwathnani H, Alonazi MA, Zhang J, Zhang L, Xing S, Yang W (2025a) Silicon enhanced phytoextraction of Sedum alfredii Hance by improving growth, Cd tolerance, and remolding rhizospheric properties. Plant Soil 512(1–2):819–836. https://doi.org/10.1007/s11104-024-07133-4
67. Xu Z, Lu H, Li S, Ma Y, Wang Y, Li R, Yang X, Huang B, Zhang H, Pan X (2025b) Integrating biochar, microbe, and hyperaccumulator for sustainable remediation of soils contaminated with heavy metals. Environ Rev 33:1–19. https://doi.org/10.1139/er-2025-0157
68. Yan H, Zhu X, Dai F, He Y, Jing X, Song P, Wang R (2021) Porous geopolymer based eco-friendly multifunctional slow-release fertilizers for promoting plant growth. Colloids Surf Physicochem Eng Asp 631:127646. https://doi.org/10.1016/j.colsurfa.2021.127646
69. Yan J, Shi L, Sang W, Yuan J, Ding D, Xia K (2026) Simultaneous enhancement of humic substances and mineral availability in weathered coal via hydrothermal modification for acid soil amendment. Sustain Mater Technol 47:e01862. https://doi.org/10.1016/j.susmat.2026.e01862
70. Yao L, Shan G, Laiba A, Zhao Y, Zhang Y, Chi R, Long B, Li W, Zhang J (2025) Fluoride species conversion-enhanced selective extraction: A green and safe strategy for fluorine recovery in wet-process phosphoric acid production. J Environ Chem Eng 13(6):119345. https://doi.org/10.1016/j.jece.2025.119345
71. Zeng A, Shi X, Zhang H, Zou Q, Ding Y, Duan H, Yang J (2026) Can phosphogypsum utilization in China be sustainable? An integrated life cycle environmental and economic evaluation. J Environ Manage 402:129095. https://doi.org/10.1016/j.jenvman.2026.129095
72. Zhang R, Liu Z, Yuan L, Wen T, Yu J (2025a) MAX-ceramic phase: A novel healing agent for resolving porosity and cracks in one-step magnesite sintering. Ceram Int 51(18):24823–24832. https://doi.org/10.1016/j.ceramint.2025.03.164

73. Zhang W, Zhao P, Pu T, Bao W, Qie H, Tan X, Ren M, Lin A (2025b) Enhancing heavy metal immobilization in cropping systems via modified clay minerals: A machine learning- assisted meta-analysis. J Environ Chem Eng 13(6):119684. https://doi.org/10.1016/j.jece.2025.119684
74. Zhang Z, Chen K, Li J, Du P, Ren J (2025c) Colloid mediated redistribution of metal species during alkaline regulation of bauxite residue: pH-dependent mobilization-immobilization dualities. J Clean Prod 533:147035. https://doi.org/10.1016/j.jclepro.2025.147035
75. Zhao Y, Lin M, Yao G, Wang S, Wang Y, Zhao Y, Wang L, Wanghan J, Cen Q, Li B, Liu Z (2026) Valorization of phosphogypsum and desulfurization gypsum via thermochemical technologies: A critical review. J Anal Appl Pyrolysis 196:107722. https://doi.org/10.1016/j.jaap.2026.107722
76. Zheng H, Yang Y, Liu W, Zhong Y, Cao Y, Qiu R, Liu C, Van Der Ent A, Hodson MJ, Tang Y (2023) Rare earth elements detoxification mechanism in the hyperaccumulator Dicranopteris linearis: [silicon-pectin] matrix fixation. J Hazard Mater 452:131254. https://doi.org/10.1016/j.jhazmat.2023.131254
77. Zhong X, Fu Y, Yu G, Jiang P, You S, Liu J (2025) Mechanisms activating trace heavy metals in the rhizosphere microenvironment of *Amaranthus hypochondriacus* L. Environ Exp Bot 229:106067. https://doi.org/10.1016/j.envexpbot.2024.106067
78. Zhou H, Jia J, Ma D, Dai L, Liu S, Liu X, Miao Y, Shu X (2025a) Thermo–chemical coupled activation of multisource solid waste for silicon fertilizer preparation. J Environ Manage 394:127385. https://doi.org/10.1016/j.jenvman.2025.127385
79. Zhou X, Xia R, Zhong J, Liu X, Xia T, Tang Y, Yang Q, Bao E, Cao K, Chen Q, He Z (2025b) Silicon and iron co-application modulates cadmium accumulation and cell wall composition in tomato seedlings. BMC Plant Biol 25(1):1001. https://doi.org/10.1186/s12870-025-06915-x
80. Zhou Q, Ma X, Hu S, Hao S, Rao Y, Wang C, Bai Q, Hu P, Liu W, Wang J (2026) Waste-derived dual-functional hierarchical magnesium silicate/diatomite composite for efficient silicon release and cadmium adsorption. Appl Clay Sci 285:108158. https://doi.org/10.1016/j.clay.2026.108158

Figures

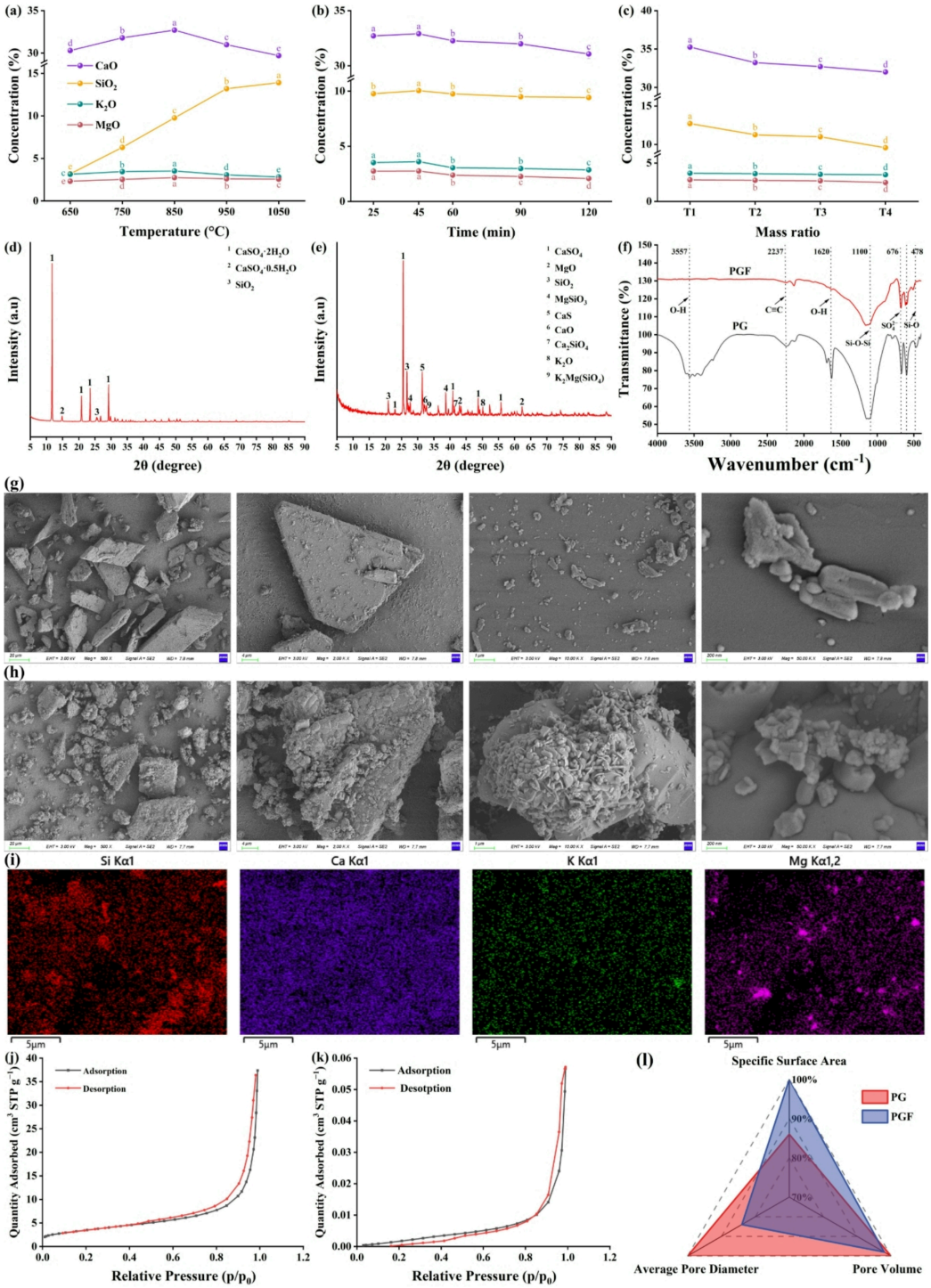


Figure 1

Optimization of the preparation process of PGF and its microstructural and phase characterization.

(a-c) Effects of calcination temperature, time, and material ratio on the contents of SiO_2, CaO, K_2O, and MgO in the product. Different lowercase letters indicate significant differences between parameters ($p < 0.05$); (d, e) XRD patterns of PG and PGF; (f) FTIR spectra of PG and PGF; (g, h) SEM morphological

images of PG and PGF; (i) EDS elemental mapping of PGF; (j, k) N_2 adsorption-desorption isotherms of PG and PGF; (l) Comparison of specific surface area, average pore diameter, and total pore volume between PG and PGF. PG: phosphogypsum; PGF: Si-Ca-K-Mg fertilizer.

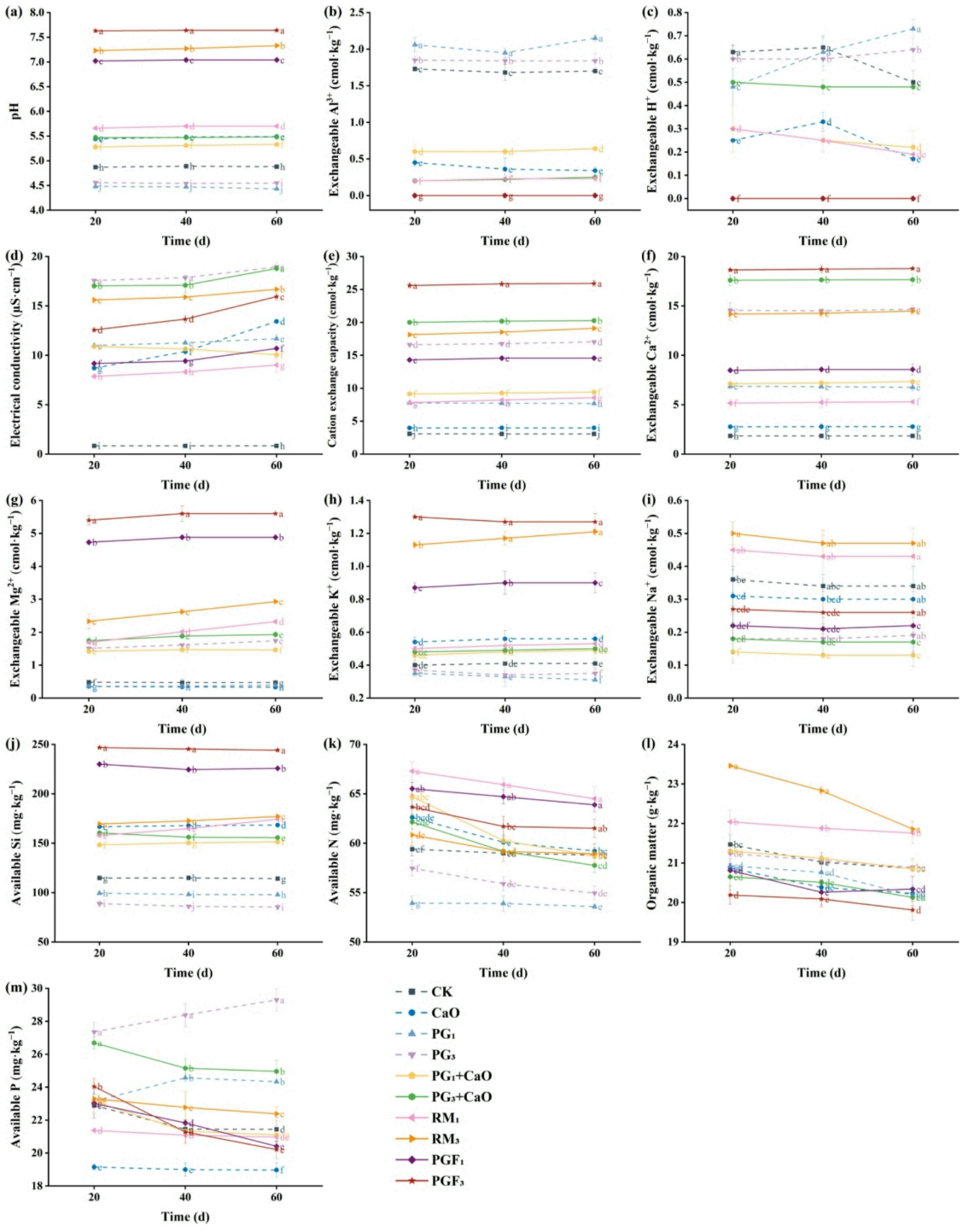


Figure 2

Effects of different treatments on soil physicochemical properties (60 d of incubation).

(a) pH; (b) Exchangeable Al^{3+}; (c) Exchangeable H^{+}; (d) Electrical conductivity (EC); (e) Cation exchange capacity (CEC); (f-i) Exchangeable base cations: (f) Ca^{2+}, (g) Mg^{2+}, (h) K^{+}, (i) Na^{+}; (j) Available Si; (k) Available N; (l) Organic matter; (m) Available P. Different lowercase letters indicate significant differences between treatments ($p < 0.05$). Abbreviations: CK, no amendment; CaO, 1% quicklime; PG_1, 1% phosphogypsum; PG_3, 3% phosphogypsum; PG_1+CaO, 1% phosphogypsum + 1% quicklime; PG_3+CaO, 3% phosphogypsum + 1% quicklime; RM_1, 1% uncalcined raw materials mixture; RM_3, 3% uncalcined raw materials mixture; PGF_1, 1% Si-Ca-K-Mg fertilizer; PGF_3, 3% Si-Ca-K-Mg fertilizer.

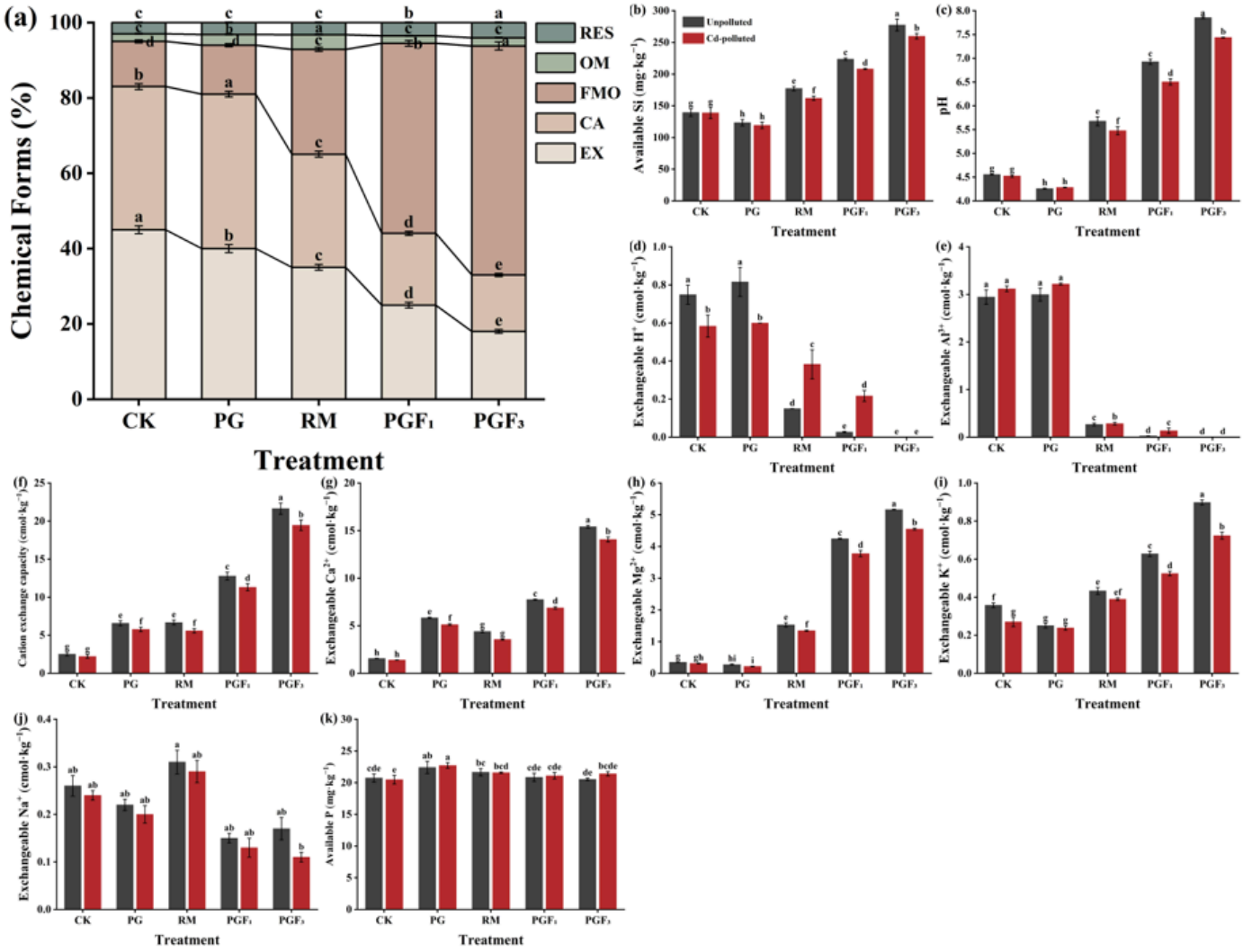


Figure 3

Comparison of soil Cd speciation distribution and physicochemical properties in the pot experiment.

(a) Chemical speciation distribution of soil Cd: Exchangeable fraction (EX), Carbonate-bound fraction (CA), Fe-Mn oxide-bound fraction (FMO), Organic matter-bound fraction (OM), Residual fraction (RES); (b) Available Si; (c) pH; (d) Exchangeable H^{+}; (e) Exchangeable Al^{3+}; (f) Cation exchange capacity (CEC); (g-j)

Exchangeable base cations: (g) Ca^{2+}, (h) Mg^{2+}, (i) K^{+}, (j) Na^{+}; (k) Available P. Different lowercase letters indicate significant differences between treatments ($p < 0.05$). Abbreviations: CK, no amendment; PG_1, 1% phosphogypsum; RM_1, 1% uncalcined raw materials mixture; PGF_1, 1% Si-Ca-K-Mg fertilizer; PGF_3, 3% Si-Ca-K-Mg fertilizer.

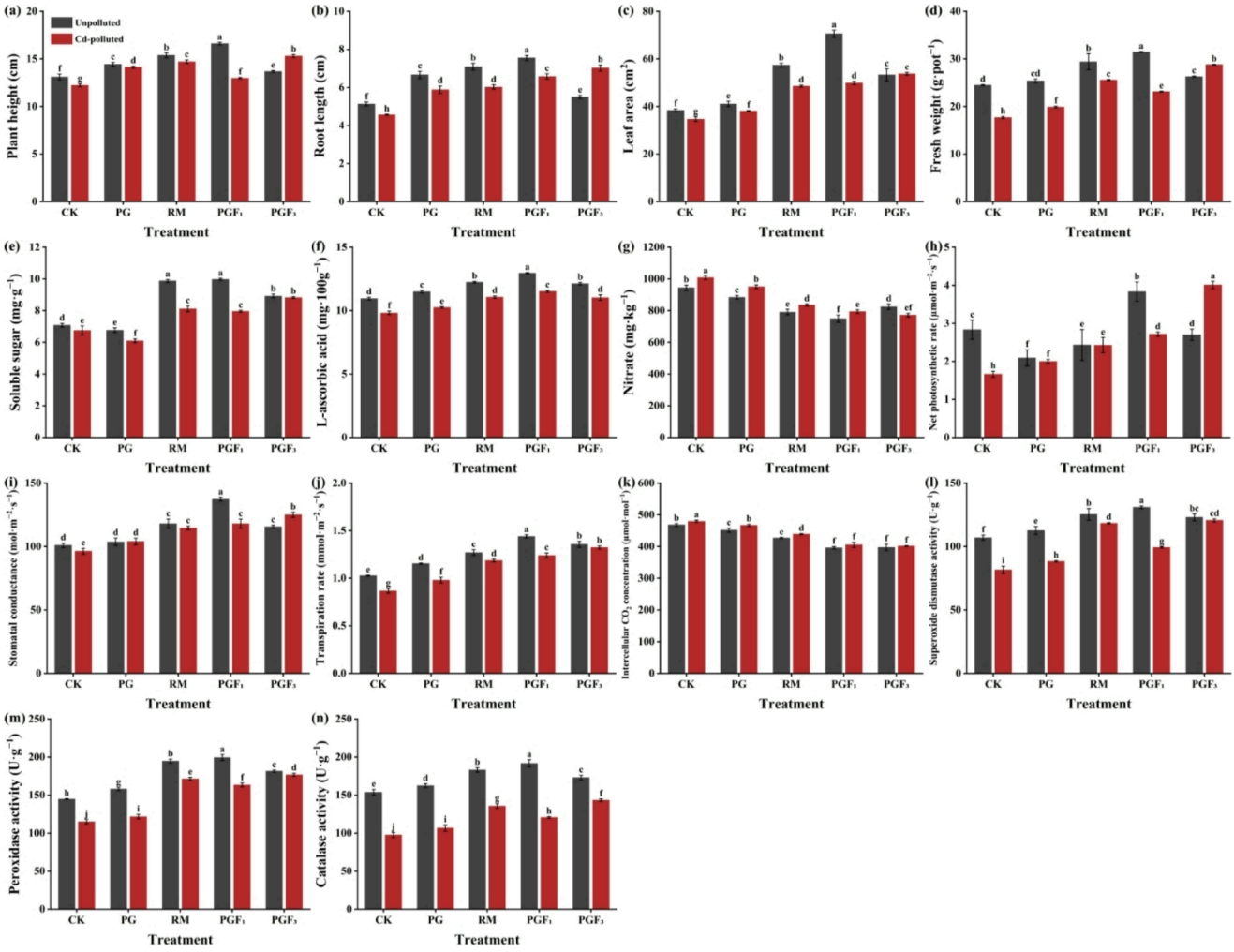


Figure 4

Effects of PGF on lettuce growth, nutritional quality, photosynthetic characteristics, and antioxidant system.

(a) Plant height; (b) Root length; (c) Leaf area; (d) Fresh weight; (e) Soluble sugar; (f) L-ascorbic acid; (g) Nitrate; (h) Net photosynthetic rate (P_n); (i) Stomatal conductance (g_s); (j) Transpiration rate (E); (k) Intercellular CO_2 concentration (C_i); (l) Superoxide dismutase activity (SOD); (m) Peroxidase activity (POD); (n) Catalase activity (CAT). Different lowercase letters indicate significant differences between

treatments ($p < 0.05$). Abbreviations: CK, no amendment; PG_1, 1% phosphogypsum; RM_1, 1% uncalcined raw materials mixture; PGF_1, 1% Si-Ca-K-Mg fertilizer; PGF_3, 3% Si-Ca-K-Mg fertilizer.

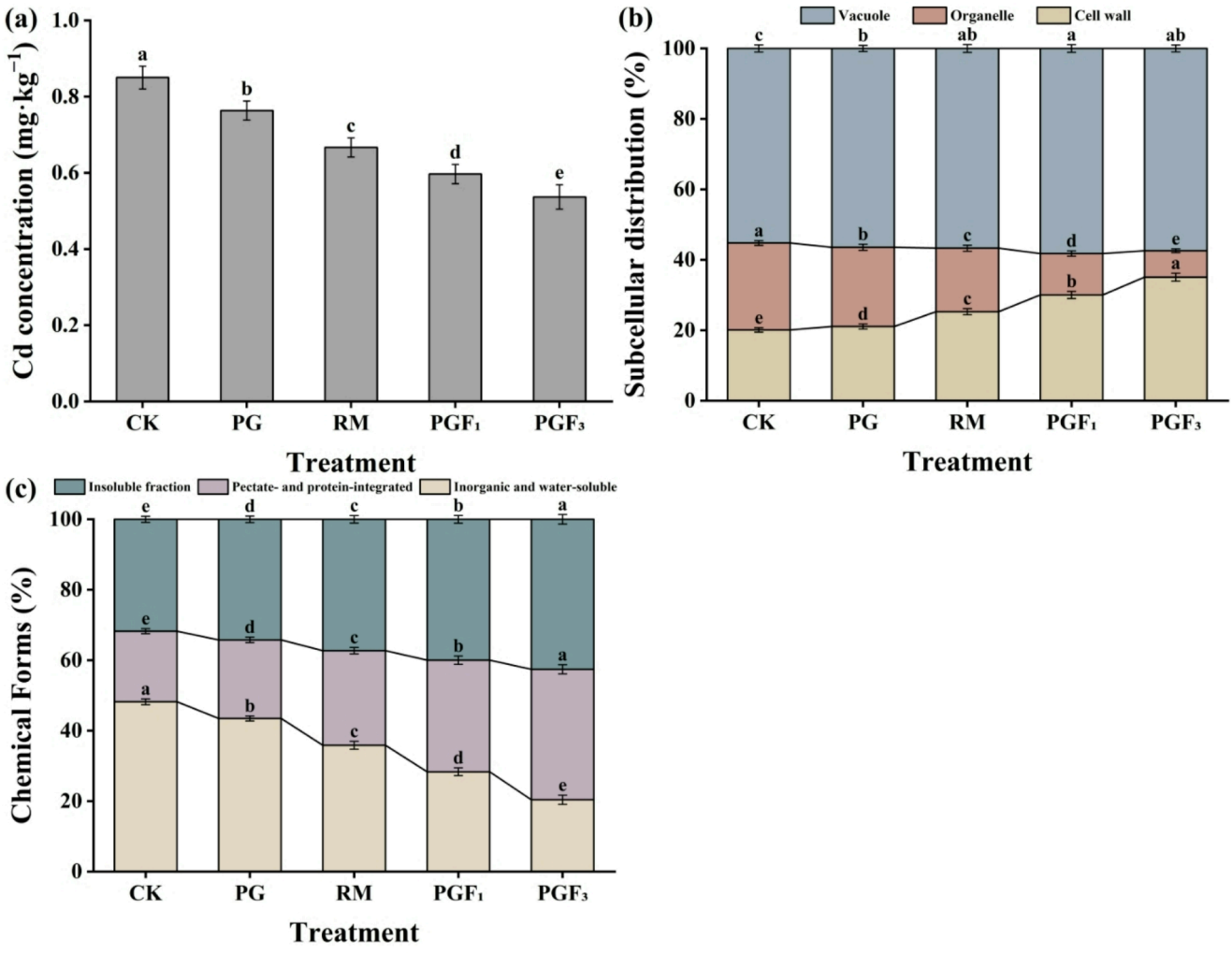


Figure 5

Accumulation characteristics, subcellular distribution, and chemical speciation transformation of Cd in lettuce.

(a) Total Cd concentration in lettuce shoots; (b) Proportion of subcellular distribution of Cd; (c) Proportion of chemical speciation of Cd. Different lowercase letters indicate significant differences between treatments ($p < 0.05$). Abbreviations: CK, no amendment; PG_1, 1% phosphogypsum; RM_1, 1% uncalcined raw materials mixture; PGF_1, 1% Si-Ca-K-Mg fertilizer; PGF_3, 3% Si-Ca-K-Mg fertilizer.

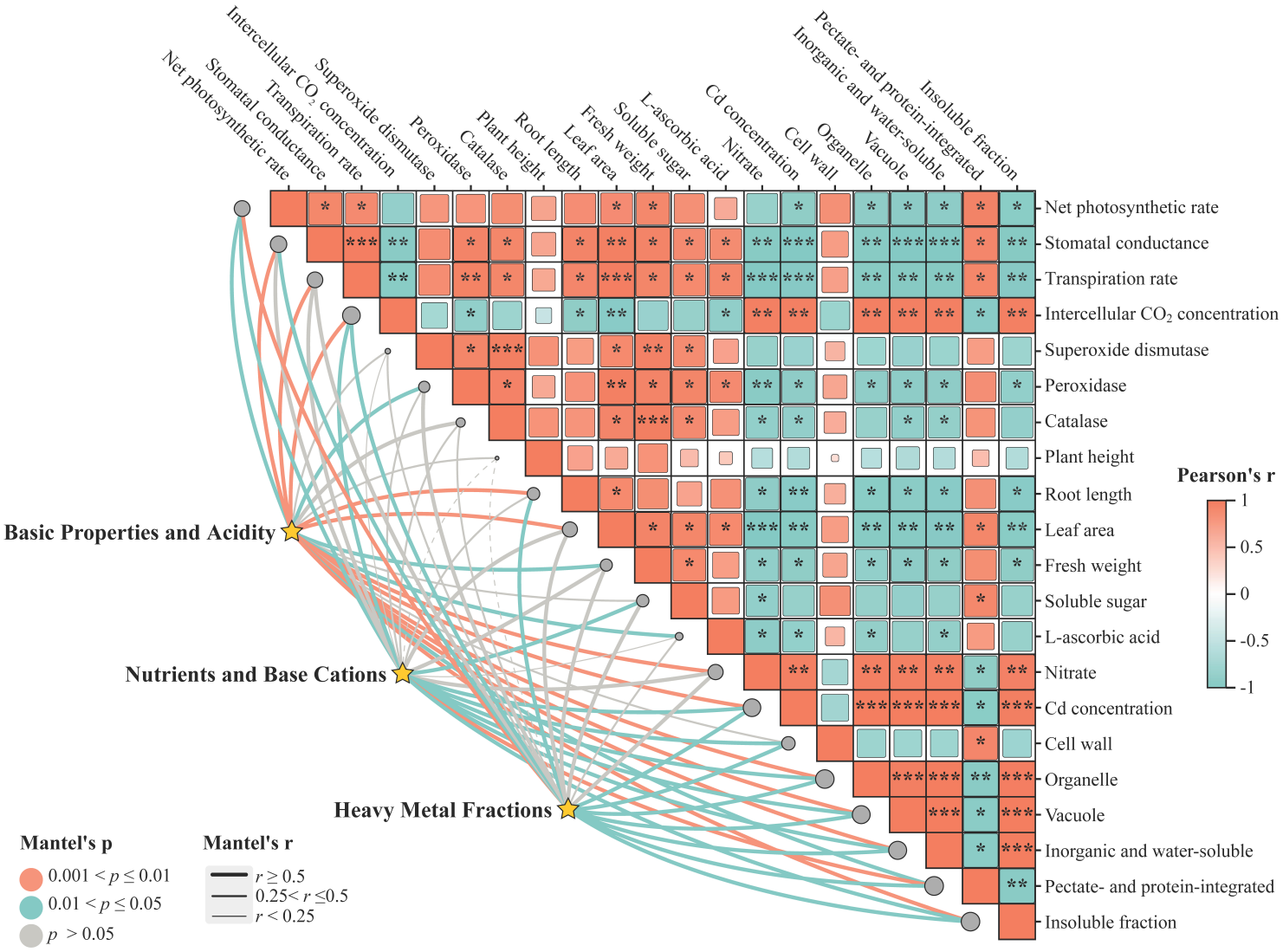


Figure 6

Mantel Test and Pearson correlation analysis between soil environmental factors and lettuce physiological indicators.

The heatmap in the lower right corner displays the Pearson correlation coefficients (r) among various lettuce indicators, with blue-green and orange-red representing negative and positive correlations, respectively. Asterisks denote significance (*$p < 0.05$, ** $p < 0.01$, *** $p < 0.001$). The lines on the left indicate the Mantel Test correlations between 3 categories of soil environmental factors and lettuce physiological indicators: line color distinguishes the significance level (Mantel's p), with orange, green, and gray representing highly significant ($p \le 0.01$), significant ($0.01 < p \le 0.05$), and not significant ($p > 0.05$), respectively; line thickness reflects correlation intensity (Mantel's r), with thick, medium, and thin lines corresponding to $r \ge 0.5$, $0.25 \le r < 0.5$, and $r < 0.25$, respectively. Soil environmental factors are categorized as follows: Basic Properties and Acidity include pH, exchangeable Al^{3+}, exchangeable H^{+}, EC, CEC, and organic matter; Nutrients and Base Cations include Available Si, Available N, Available P, and exchangeable Ca^{2+}, Mg^{2+}, K^{+}, Na^{+}; Heavy Metal Fractions include the exchangeable fraction (EX),

carbonate-bound fraction (CA), Fe-Mn oxide-bound fraction (FMO), organic matter-bound fraction (OM), and residual fraction (RES) of soil Cd.

Supplementary Files

This is a list of supplementary files associated with this preprint. Click to download.

- Supplementarymaterial.docx
- floatimage1.png